

A practical determination strategy of optimal threshold
parameter for matrix compression in wavelet BEM

Kazuhiro Koro, Kazuhisa Abe*

*Department of Civil Engineering and Architecture,
Niigata University*

8050 Igarashi 2-Nocho, Niigata, 950-2181, JAPAN

*Corresponding author, Fax; +81-25-262-7021, E-mail; abe@eng.niigata-u.ac.jp

Summary

A practical strategy is developed to determine the optimal threshold parameter for wavelet-based BE analysis. The optimal parameter is determined so that the amount of storage (and computational work) is minimized without reducing the accuracy of BE solution. In the present study, the Beylkin-type truncation scheme is used in the matrix assembly. To avoid unnecessary integration concerning the truncated entries of a coefficient matrix, *a priori* estimation of the matrix entries is introduced and thus the truncated entries are determined twice: before and after matrix assembly. The optimal threshold parameter is set based on the equilibrium of the truncation and discretization errors. These errors are estimated in the residual sense. For Laplace problems the discretization error is in particular, indicated with the potential's contribution $\|\mathbf{c}\|$ to the residual norm $\|\mathbf{R}\|$ used in error estimation for mesh adaptation. Since the normalized residual norm $\|\mathbf{c}\|/\|\mathbf{u}\|$ (\mathbf{u} : the potential components of BE solution) cannot be computed without main BE analysis, the discretization error is estimated by the approximate expression constructed through subsidiary BE calculation with smaller degree of freedom (DOF). The matrix compression using the proposed optimal threshold parameter enables us to generate a sparse matrix with $O(N^{1+\gamma})$ ($0 \leq \gamma < 1$) non-zero entries. Although the quasi-optimal memory requirements and complexity are not attained, the compression rate of a few percent can be achieved for $N \sim 1,000$.

Key Words

wavelet BEM, truncation, optimal threshold parameter, non-orthogonal spline wavelet

1 Introduction

In engineering applications of the boundary element method (BEM), the system of N algebraic equations (N : degree of freedom) derived through the discretization of a boundary integral equation (BIE) has a dense $N \times N$ coefficient matrix. Such a matrix obviously requires $O(N^2)$ amount of storage. Besides, the computational work for solving the algebraic equations grows with $O(N^3)$ and $O(N^2)$ for direct and iterative solvers, respectively. These properties make it difficult to apply the BEM to large-scale problems. To overcome this obstacle, the effective techniques for reducing the computational cost have been developed over the last decade: a wavelet-based boundary element method (wavelet BEM, e.g., [1][2][3][4]) and a fast multipole method (FMM, e.g., [5][6]) are major fast methods for BE analysis.

In the wavelet BEM, wavelets, with which a function can be represented on various resolution levels, are employed as the basis functions for discretizing a BIE. In this situation, the entries of the coefficient matrix are generated through evaluation of the single- or double integrals including the wavelets. Moreover, the matrix entries have a faster decay on the distance between two supports of the bases than that in conventional BE analysis. This is due to the local support and vanishing moment properties of wavelets. As a result, most of the matrix coefficients, in particular the far-field influences in the entries, have small value relatively to the entries populated around matrix diagonal. We can thus assemble a sparse coefficient matrix by truncating these small entries of the original fully-populated one.

The wavelet BEM however, has some difficulties on its engineering application. One is that it is difficult to generate surface wavelets suitable for 3-D BE analysis. Many surface wavelets are hence defined by tensor products of univariable wavelets (e.g., [2]). Otherwise we have to use the multiwavelet [8] that enables us to implement triangulation of surfaces; this wavelet has the discontinuity of polynomials on the supports. Another is that one needs to determine the thresholding value for the truncation of small entries in advance. In the present stage of engineering applications of the wavelet methods, the wavelet algorithm with the complexity of $O(N)$ has been proposed [9]; in general it is difficult to develop the wavelet methods comparable to the FMM. Many researchers thus recognize that the wavelet BEM is hard to apply the practical large-scale problems like 3-D problems in contrast to FMM algorithms. However, the basic idea of the wavelet methods is comparatively simple; the wavelet BEM can readily reduce the computational cost by only using the wavelets as the basis functions. Hence, this approach can become one of the choices for the cost reduction for BE analysis.

As stated above, in wavelet-based BE analysis a sparse matrix is generated by truncating small matrix entries. The truncation, which is to replace smaller entries than prescribed thresholding value by null entries, is an important technique to reduce the cost of the wavelet BEM. Obviously, the use of large thresholding value is effective for memory reduction. In matrix assembling, when the *a priori*-type truncation schemes (e.g., [3]) are used, the boundary integrals on the truncated entries are not calculated. Then, we can

shorten the CPU time remarkably. However, the matrix compression with an extremely large threshold incurs the accuracy reduction in BE solution. We therefore, have to use the truncation strategies that reduce the computational cost as much as possible with sustaining the accuracy.

The truncation strategy preserving the accuracy of BE solution has been utilized in mathematical and numerical analysis by Dahmen et al. [7], Schneider [9], Schwab and his co-researchers [3][8][10][11] and Rathsfeld [2]. In this strategy the truncation is carried out so that the rate of asymptotical convergence of the BE solution is not affected by the matrix compression. To preserve the convergence rate, the truncation is carried out using the thresholding values dependently on the resolution levels of wavelets. As a result, we can reduce the amount of storage and the computational work to $O(N(\log N)^a)$ ($a \geq 0$). In this compression scheme, the magnitude of the thresholding value is controlled with several truncation parameters: those are determined through theoretical estimations and subsidiary computations with lower DOFs.

In many engineering applications, the truncation algorithm proposed by Beylkin et al. [12], which is the alternative of the above Dahmen-Schwab matrix compression scheme (e.g., [4], [13], [14], [15]). The Beylkin-type truncation scheme enables us to reduce the memory requirements to $O(N \log N)$ using a fixed threshold parameter independently of the DOF. Although this method has a simple criterion and the truncation is carried out under a threshold irrespective of the wavelet level, the determination method of the optimal thresholding value has not been developed.

In the present paper, we develop a practical strategy for determining the threshold parameter used in the Beylkin-type matrix compression scheme. We target to determine, in particular, the optimal threshold parameter, by which the matrix compression minimizes the number of stored entries with preserving the accuracy of BE solution. To determine such optimal value, we allow the truncation error in BE solution up to the level comparable to the discretization error. Hence, the optimal threshold parameter obviously has problem dependency, and consequently, its value varies with the boundary conditions, the degree of interpolation and the DOFs. In particular, the optimal value depends on DOF, even if the boundary conditions and the degree of interpolation remain unchanged. We derive the estimation of the optimal threshold parameter based on the equilibrium of the truncation and discretization errors. These errors are estimated in the residual sense, in particular, the discretization error is indicated with the residual \mathbf{R} , which is used in error estimation in adaptive meshing [18][19]. As a result, the estimated value shows $O(N^{-\beta})$ where β is the asymptotical order of the potential's contribution $\|\mathbf{c}\|$ to the residual norm $\|\mathbf{R}\|$. By taking the dependence on the DOF into account and introducing further several assumptions and approximations, the optimal threshold can be estimated from its approximate expression constructed through computations with smaller DOFs than that on main BE analysis, like the Dahmen-Schwab compression scheme. The validity and justification of these assumptions and approximations will be verified below through numerical tests.

As stated above, the matrix compression based on the Beylkin-type algorithm results

in $O(N \log N)$ amount of storage using a fixed thresholding value. However, we utilize the optimal threshold parameter that depends on the DOF. When using such optimal value, we cannot unfortunately obtain the memory requirements of quasi-linear order: the number of non-zero entries has $O(N^{1+\gamma})$ ($0 \leq \gamma < 1$). Although this asymptotical order is not as good as that for Dahmen-Schwab matrix compression of $O(N(\log N)^a)$ complexity, the compression rates of coefficient matrix are reduced to a few percent for about 1,000 DOFs, as will be shown in Section 6. Through these results, we can find that the matrix compression using the present algorithm is sufficiently effective for the reduction of memory requirements and computational work.

The present paper is organized as follows: in Section 2, we summarize implementation of the wavelet BEM using the non-orthogonal spline wavelets. These wavelets developed by the authors [4] have several properties suitable for BE analysis. Section 3 contains the estimation of the discretization- and truncation errors in BE solution. The details of the present determination strategy, which is developed based on the error estimations, are described in Section 4. In Section 5, we estimate the number of non-zero entries of the matrix that is compressed with the Beylkin-type algorithm and using the optimal threshold parameter. In Section 6, the numerical experiments on 2-D Laplace problems are undertaken to verify the numerical manipulations in the present strategy. We also demonstrate the Beylkin-type matrix compression using the optimal threshold parameter through the test examples. Finally, the concluding remarks on the present study are summarized in Section 7.

2 Wavelet BEM

2.1. Wavelets

In the wavelet BEM, the solution of a boundary integral equation is approximated by wavelet series. The wavelet series consist of two kinds of basis functions: a scaling function ϕ and a wavelet ψ . These basis functions are defined as the bases of the following subspaces \mathbf{V} and \mathbf{W} in the Hilbert space $L^2[0, 1]$:

$$\mathbf{V}_0 \subset \mathbf{V}_1 \subset \mathbf{V}_2 \subset \cdots \subset \mathbf{V}_k \subset \cdots \subset L^2[0, 1], \quad (1)$$

$$\mathbf{V}_{k+1} = \mathbf{V}_k + \mathbf{W}_k, \quad (2)$$

$$\mathbf{V}_k = \overline{\text{span}\{\phi_{k,j} := 2^{k/2}\phi(2^k\xi - j), j = 1, 2, \dots, n_\phi^{(k)}\}}, \quad (3)$$

$$\mathbf{W}_k = \overline{\text{span}\{\psi_{k,j} := 2^{k/2}\psi(2^k\xi - j), j = 1, 2, \dots, n_\psi^{(k)}\}}, \quad (4)$$

where $n_\phi^{(k)}$ is the number of the bases $\phi_{k,j}$ with resolution level k , and $n_\psi^{(k)} = n_\phi^{(k+1)} - n_\phi^{(k)}$.

From equations (1) and (2), the space $L^2[0, 1]$ can be decomposed into a direct sum of \mathbf{V}_0 and \mathbf{W} at every resolution, that is,

$$L^2[0, 1] = \mathbf{V}_0 + \bigcup_{k=0}^{\infty} \mathbf{W}_k. \quad (5)$$

This relation ensures that a function f in $L^2[0, 1]$ can be represented using the basis

functions of the subspaces. Hence, we can obtain the following expression as the wavelet expansion of the function f :

$$f(\xi) = \sum_{j=1}^{n_s} \hat{f}_{0,j} \phi_{0,j}(\xi) + \sum_{k=0}^{\infty} \sum_{j=1}^{n_w} \tilde{f}_{k,j} \psi_{k,j}(\xi), \quad (6)$$

where $\hat{f}_{0,j}$ and $\tilde{f}_{k,j}$ are the expansion coefficients corresponding to $\phi_{0,j}$ and $\psi_{k,j}$. n_s and n_w are equal to $n_\phi^{(0)}$ and $n_\psi^{(k)}$, respectively.

In equation (6), truncating the summation with respect to k up to prescribed resolution level M , we obtain the projection $P_{M+1}f(\xi) \in \mathbf{V}_{M+1}$ as an approximation of the function f . i.e.,

$$f(\xi) \simeq P_{M+1}f(\xi) := \sum_{j=1}^{n_s} \hat{f}_{0,j} \phi_{0,j}(\xi) + \sum_{k=0}^M \sum_{l=1}^{n_w} \tilde{f}_{k,l} \psi_{k,l}(\xi). \quad (7)$$

Many kinds of wavelets used in equations (6) and (7) have been developed. In the present stage of application of the wavelet BEM to engineering analyses, the Chui's semi-orthogonal wavelets [1][10], several orthonormal wavelets [13][14][15][16] and the non-orthogonal wavelets developed by the authors [4] have been used in 2-D BE analysis. Moreover, the multiwavelets are available for 3-D problems, which has been shown by e.g., Schwab et al. [3][8]. In the present study, we define wavelet series (7) using the B-spline ϕ^m and the non-orthogonal spline wavelet ψ_n^m . These basis functions possess the properties suitable for BE analysis: these have closed forms and compact supports. The scaling function and the wavelet are defined as follows [4]:

$$\phi(\xi) = \phi^m(\xi) = \frac{1}{m!} \sum_{j=0}^{m+1} (-1)^j \binom{m+1}{j} (\xi - j)_+^m = \frac{1}{2^m} \sum_{j=0}^{m+1} \binom{m+1}{j} \phi(2\xi - j), \quad (8)$$

$$\psi(\xi) = \psi_n^m(\xi) = \frac{\alpha_n^m}{m!} \sum_{j=0}^{m+n+1} (-1)^j \binom{m+n+1}{j} (2\xi - j)_+^m = \alpha_n^m \sum_{j=0}^n (-1)^j \binom{n}{j} \phi(2\xi - j), \quad (9)$$

where α_n^m is the constant to normalize $\psi(\xi)$ on the intrinsic coordinates ξ , and $(\cdot - j)_+^m$ represents the truncated power function of degree m . n is the order of vanishing moments;

$$\int_{-\infty}^{\infty} \xi^k \cdot \psi(\xi) d\xi = 0, \quad (k = 0, 1, \dots, n-1). \quad (10)$$

In BE analysis, we can generate a larger number of small matrix entries using wavelets with higher-order vanishing moments, and then we can obtain a sparser coefficient matrix by truncating the small entries [4][12]. The non-orthogonal wavelet (9) allows us to choose the order of the vanishing moments independently of the degree of polynomials m . This is an important characteristic of the non-orthogonal wavelets on BE analysis. On the other hand, the accepted wisdom is that the choice of a higher-order of vanishing moments is not always advantageous for reduction of computational work: Lage and Schwab [3] have argued that the asymptotical complexity is almost optimal using the wavelets with

a minimal number of vanishing moments (e.g., Haar wavelet). This view is based on the fact that the number of subintervals of the spline wavelets increases linearly with the order of vanishing moments. A matrix entry concerning the wavelets with many subintervals is calculated costly, in particular through numerical integration with the conventional Gauss-Legendre formula; the amount of this computational cost can be reduced with the wavelet-weighted Gaussian quadrature formulae [17].

The wavelet series using basis functions (8) and (9) however, have no completeness on a finite interval. This is because the basis arranged at the ends on the interval has a truncated support. To ensure the completeness of the wavelet expansion, we introduce the special basis functions. These are referred to as *boundary scaling function* or *boundary wavelet*.

The boundary scaling function $\bar{\phi}_i^m$ is given by the B-spline with a multiple knot at the truncated point of the support, whereas the boundary wavelet $\bar{\psi}_i$ is defined by

$$\bar{\psi}_i(\xi) = \bar{\psi}_{in}^m(\xi) = \begin{cases} \psi_{n+i}^0(\xi) & (m = 0) \\ \bar{\alpha}_{i1}^m [\bar{\phi}_1^m(2\xi) + p_i \cdot \bar{\phi}_{i+1}^m(2\xi)] & (i < m, m \geq 1, n = 1) \\ \bar{\alpha}_{i1}^m [\bar{\phi}_1^m(2\xi) + p_i \cdot \phi^m(2\xi)] & (i = m, m \geq 1, n = 1) \\ \bar{\alpha}_{in}^m [\bar{\psi}_{1(n-1)}^m(\xi) + a_{i,n-1} \cdot \psi_{n-1}^m(\xi)] & (i \leq m, m \geq 1, n \geq 2) \end{cases} \quad (11)$$

where $\bar{\alpha}_n^m$ is the constant normalizing $\bar{\psi}_i$. The constant p_i is set to such value as $\bar{\psi}_{i1}^m$ satisfies the first-order vanishing moment condition, and $a_{i,n-1}$ is evaluated by

$$a_{i,n-1} = - \frac{\int_0^\infty \xi^{n-1} \bar{\psi}_{i1}^m(\xi) d\xi + \sum_{j=1}^{n-2} a_{i,j} \int_0^\infty \xi^{n-1} \psi_j^m(\xi) d\xi}{\int_0^\infty \xi^{n-1} \psi_{n-1}^m(\xi) d\xi}. \quad (12)$$

where $\alpha_0^m = a_{i,0} = 0$.

In definition of the wavelet expansion on a finite interval, the basis functions with truncated supports are replaced by the boundary bases $\bar{\phi}_i^m$ and $\bar{\psi}_i$. Then, we have to choose the wavelets of $m + n = (\text{odd})$, in order to preserve symmetry of expanded functions.

2.2. Boundary element equations

Let us now consider 2-D Laplace problems, which are described by the following BIE:

$$c(\mathbf{x})u(\mathbf{x}) + \int_\Gamma q^*(\mathbf{x}, \mathbf{y})u(\mathbf{y}) d\Gamma_y - \int_\Gamma u^*(\mathbf{x}, \mathbf{y})q(\mathbf{y}) d\Gamma_y = 0, \quad (\mathbf{x}, \mathbf{y} \in \Gamma), \quad (13)$$

where u and q are the potential and its outward normal derivative on the boundary Γ , respectively. The kernel functions u^* and q^* are the fundamental solutions corresponding to u and q . $c(\mathbf{x})$ is the free term.

To derive the system of equations from the BIE, we introduce the approximations \tilde{u} and

\tilde{q} defined by the following wavelet series:

$$\begin{aligned}\tilde{u} &= \sum_{i=1}^N \tilde{U}_i w_i = \sum_{j=1}^{n_s} \hat{u}_{0,j} \phi_{0,j} + \sum_{k=0}^{m_r} \sum_{l=1}^{n_k} \tilde{u}_{k,l} \psi_{k,l}, \\ \tilde{q} &= \sum_{i=1}^N \tilde{Q}_i w_i = \sum_{j=1}^{n_s} \hat{q}_{0,j} \phi_{0,j} + \sum_{k=0}^{m_r} \sum_{l=1}^{n_k} \tilde{q}_{k,l} \psi_{k,l}.\end{aligned}\tag{14}$$

where n_s and n_k are the number of the scaling functions $\phi_{0,j}$ and the wavelets $\psi_{k,l}$, respectively. The bases $\{w_i\}$ ($i = 1, \dots, N$) consist of all the scaling functions and the wavelets used in equation (14). $\hat{u}_{0,j}$, $\tilde{u}_{k,l}$, $\hat{q}_{0,j}$ and $\tilde{q}_{k,l}$ are the expansion coefficients. Moreover, N is the degree of freedom, and m_r is the finest resolution level.

In equation (13), the replacement of u and q by \tilde{u} and \tilde{q} yields the following residual r :

$$r(\mathbf{x}) := c(\mathbf{x})\tilde{u}(\mathbf{x}) + \int_{\Gamma} q^*(\mathbf{x}, \mathbf{y})\tilde{u}(\mathbf{y}) d\Gamma_y - \int_{\Gamma} u^*(\mathbf{x}, \mathbf{y})\tilde{q}(\mathbf{y}) d\Gamma_y.\tag{15}$$

We now apply the Galerkin method to equation (15): we require to satisfy with

$$\int_{\Gamma} r \cdot w_i d\Gamma = 0, \quad (i = 1, 2, \dots, N).\tag{16}$$

In the wavelet BEM, the BIE is usually discretized by the Galerkin method. Although we can use the collocation method for the discretization, we have to perform special algorithm (e.g., the fast wavelet transformation: FWT) to the coefficient matrix derived by the collocation scheme [2][7][16], in order to obtain the computational performance comparable to that of the Galerkin scheme.

From equations (14), (15) and (16), we obtain a system of algebraic equations as follows:

$$\mathbf{H}\mathbf{u} = \mathbf{G}\mathbf{q},\tag{17}$$

where the components of the vectors \mathbf{u} and \mathbf{q} are the expansion coefficients \tilde{U}_i and \tilde{Q}_i , respectively. The matrices \mathbf{G} and \mathbf{H} are assembled through evaluation of the following single- and double integrals:

$$\begin{aligned}g_{ij} &= \int_{\Gamma_i} w_i \int_{\Gamma_j} u^* w_j d\Gamma^2, \\ h_{ij} &= \frac{1}{2} \int_{\Gamma_i} w_i w_j d\Gamma + \int_{\Gamma_i} w_i \int_{\Gamma_j} q^* w_j d\Gamma^2, \quad (i, j = 1, 2, \dots, N).\end{aligned}\tag{18}$$

Note that g_{ij} and h_{ij} denote the entries of \mathbf{G} and \mathbf{H} .

Taking account of boundary conditions, we consequently obtain the following linear equation:

$$\mathbf{A}\mathbf{z} = \mathbf{B}\bar{\mathbf{y}} = \mathbf{b},\tag{19}$$

where \mathbf{A} and \mathbf{B} are the coefficient matrices corresponding to the unknown vector \mathbf{z} and the known vector $\bar{\mathbf{y}}$, respectively. In implementation of the wavelet-based BE analysis, we have to evaluate the known expansion coefficients $\bar{\mathbf{y}}$. This computation requires the inversion of the $N \times N$ matrix; we can perform the computation at $O(N)$ operations using the FWT algorithm [4].

2.3. Truncation strategy

As mentioned above, we truncate the small entries of the coefficient matrix using the Beylkin-type algorithm [12]. This truncation strategy enables us to generate a sparse coefficient matrix by neglecting smaller entries than prescribed thresholding value that is independent of the level of wavelets. In matrix compression based on the Beylkin-type original scheme, we first generate all the matrix entries g_{ij} and h_{ij} by equation (18), and the truncated entries are usually selected through comparing the absolute value of the matrix entries with the thresholding value. We thus need $O(N^2)$ operations for generation of $O(N \log N)$ or $O(N^{1+\gamma})$ ($0 \leq \gamma < 1$) non-zero entries. To save the computational work, we should avoid unnecessary operations concerning the truncated entries. In the present study, we reduce the computation by determining truncated entries not only at after calculation of g_{ij} and h_{ij} , but also at before the integration.

In the stage before generating the matrix entries, we estimate the absolute value of the entries using asymptotic expansion, instead of calculating equation (18). The estimates are given by

$$|g_{ij}| \simeq \bar{g}_{ij} := C_g \cdot \frac{2^{-\frac{2n+1}{2}(k_i+k_j)}}{\bar{r}^{n(\beta_i+\beta_j)}}, \quad |h_{ij}| \simeq \bar{h}_{ij} := C_h \cdot \frac{2^{-\frac{2n+1}{2}(k_i+k_j)}}{\bar{r}^{n(\beta_i+\beta_j)+1}},$$

$$C_g := \frac{\bar{\ell}_i^{n\beta_i+1} \bar{\ell}_j^{n\beta_j+1} \{n(\beta_i + \beta_j) - 1\}!}{(m+1)^{2-\beta_i-\beta_j}} \left\{ \frac{\alpha_n^m}{(m+n+1)^{n+1}} \right\}^{\beta_i+\beta_j}, \quad C_h := C_g \cdot n(\beta_i + \beta_j),$$
(20)

where $\bar{r} := \text{dist}(\text{supp } w_i, \text{supp } w_j)$, and $\bar{\ell}$ is the support length of the scaling function ϕ_0 . The constant β is equal to 0 ($w = \phi_0$) or 1 ($w = \psi_k$). k_i and k_j are the resolution level of the bases w_i and w_j , respectively. Note that $k = 0$ for $w = \phi_0$. C_g and C_h are independent of k_i , k_j and \bar{r} , and are determined from the coefficients of the leading terms of the asymptotic series.

The truncation before generating g_{ij} and h_{ij} , namely *a priori* truncation, is carried out using estimate (20). Although the *a priori* truncation spends computational work of $O(N^2)$, the computation time for this estimation is negligible in the assembly of the matrix owing to the simple form of equation (20), as will be shown in the numerical tests. The matrix entries satisfying the following conditions are truncated without calculation of double integral (18):

$$\bar{g}_{ij} < \eta_g \cdot G_{max}, \quad \bar{h}_{ij} < \eta_h \cdot H_{max},$$
(21)

where G_{max} and H_{max} are the maximum value of $|g_{ij}|$ and $|h_{ij}|$ whose both two basis functions w_i and w_j are given by scaling functions. η_g and η_h are the threshold parameters corresponding to the matrices \mathbf{G} and \mathbf{H} , respectively. We will determine the optimal value of these parameters.

The entries over the thresholding value $\eta_g \cdot G_{max}$ or $\eta_h \cdot H_{max}$ in truncation condition (21) are evaluate by equation (18). Then, the matrix entries g_{ij} and h_{ij} satisfying

$$|g_{ij}| < \eta_g \cdot G_{max}, \quad |h_{ij}| < \eta_h \cdot H_{max},$$
(22)

are replaced by zero. We call this procedure *a posteriori* truncation.

Note that we do not apply the above truncation process to the entries satisfying: (i) $\bar{r} < (2^{-k_i} \bar{\ell}_i + 2^{-k_j} \bar{\ell}_j)$ or (ii) both bases are scaling functions.

3 Error estimation for determining optimal threshold parameter

In the present paper, we attempt to determine the optimal threshold parameter used in the Beylkin-type truncation algorithm for the wavelet BEM. As stated in Section 1, the matrix compression using the optimal thresholding value minimizes the memory requirements of stored entries with preserving the accuracy of BE solution. To determine such optimal value, the equilibrium of the truncation and discretization errors is imposed on the BE solution. We consequently have to separately estimate these errors for the optimal value setting.

3.1. Truncation error

To estimate the truncation error, let us consider boundary element equation (19). Then, the coefficient matrices obtained after the truncation, $\tilde{\mathbf{A}}$ and $\tilde{\mathbf{B}}$, are expressed as

$$\tilde{\mathbf{A}} = \mathbf{A} + \Delta\mathbf{A}, \quad \tilde{\mathbf{B}} = \mathbf{B} + \Delta\mathbf{B}, \quad (23)$$

where the matrices $\Delta\mathbf{A}$ and $\Delta\mathbf{B}$ consist of the truncated entries of \mathbf{A} and \mathbf{B} , respectively.

The truncation of the small entries of \mathbf{A} and \mathbf{B} yields an additional error $\Delta\mathbf{z}$ of the BE solution \mathbf{z} , and then boundary element equation (19) is rewritten by

$$\tilde{\mathbf{A}}(\mathbf{z} + \Delta\mathbf{z}) = \tilde{\mathbf{B}}\bar{\mathbf{y}}. \quad (24)$$

Rearranging equation (24) and then applying equation (19) to the resulting equation, we obtain the contribution $\mathbf{A}\Delta\mathbf{z}$ of the truncation error to the residual of equation (24) as follows:

$$\mathbf{A}\Delta\mathbf{z} \simeq -[\Delta\mathbf{A}]\mathbf{z} + [\Delta\mathbf{B}]\bar{\mathbf{y}} = -[\Delta\mathbf{H}]\mathbf{u} + [\Delta\mathbf{G}]\mathbf{q}, \quad (25)$$

where $\Delta\mathbf{G}$ and $\Delta\mathbf{H}$ are the matrices whose entries are the truncated ones of the matrices \mathbf{G} and \mathbf{H} , respectively. The truncation error $\Delta\mathbf{z}$ can be obtained by solving equation (25). This equation however, has the same DOF, N , as that of BE solution (14). In the stage of determination of the optimal thresholding value, the matrix \mathbf{A} is not compressed, i.e., this is an $N \times N$ fully-populated matrix. The direct estimation of $\Delta\mathbf{z}$ obviously requires larger computational work than that of main BE analysis. We thus attempt to indirectly estimate the truncation error in the residual sense.

The residual norm $\|\mathbf{A}\Delta\mathbf{z}\|$ is estimated by applying the triangle inequality to equation (25) as follows:

$$\|\mathbf{A}\Delta\mathbf{z}\| \leq \|\Delta\mathbf{H}\| \cdot \|\mathbf{u}\| + \|\Delta\mathbf{G}\| \cdot \|\mathbf{q}\|. \quad (26)$$

Substituting $\mathbf{q} = \mathbf{G}^{-1}\mathbf{H}\mathbf{u}$ in equation (26), we have

$$\frac{\|\mathbf{A}\Delta\mathbf{z}\|}{\|\mathbf{u}\|} \leq \|\mathbf{H}\| \left(\frac{\|\Delta\mathbf{H}\|}{\|\mathbf{H}\|} + \text{cond}(\mathbf{G}) \frac{\|\Delta\mathbf{G}\|}{\|\mathbf{G}\|} \right), \quad (27)$$

where $\text{cond}(\mathbf{G})$ is the condition number of the matrix \mathbf{G} .

3.2. Discretization error

Following the truncation error estimation, we now describe an approach for estimating the discretization error in the sense of residual. This estimation has to be consistent of the above truncation error estimation. We thus estimate the discretization error using the residual \mathbf{R} , which has been proposed for the error estimation in adaptive meshing scheme, by Abe [18][19].

To clarify the relation between the discretization error and the residual \mathbf{R} , let us consider the residual r defined by equation (15). The residual r is equal to a difference between equations (13) and (15), since equation (13) holds for the true solution of the BIE identically. That is,

$$-\frac{1}{2}(u - \tilde{u}) - \int_{\Gamma} q^*(u - \tilde{u}) d\Gamma + \int_{\Gamma} u^*(q - \tilde{q}) d\Gamma = r. \quad (28)$$

When applying orthogonal condition (16) to equation (28), we obtain the equations with respect to $(u - \tilde{u})$ and $(q - \tilde{q})$ as follows:

$$\frac{1}{2} \int_{\Gamma} w_i(u - \tilde{u}) d\Gamma + \int_{\Gamma} w_i \int_{\Gamma} q^*(u - \tilde{u}) d\Gamma^2 - \int_{\Gamma} w_i \int_{\Gamma} u^*(q - \tilde{q}) d\Gamma^2 = 0, \quad (29)$$

$$(i = 1, 2, \dots, N).$$

In equation (29), we rearrange $(u - \tilde{u})$ and $(q - \tilde{q})$ to

$$u - \tilde{u} = (u - \check{u}) + (\check{u} - \tilde{u}), \quad q - \tilde{q} = (q - \check{q}) + (\check{q} - \tilde{q}), \quad (30)$$

where \check{u} and \check{q} are the wavelet series corresponding to the true solutions u and q , and are given by

$$\check{u} = \sum_{i=1}^N U_i w_i, \quad \check{q} = \sum_{i=1}^N Q_i w_i, \quad (31)$$

where U_i and Q_i are the expansion coefficients of the true solutions u and q , respectively.

Substituting equations (14), (30) and (31) into equation (29), we can obtain the following algebraic equation:

$$\mathbf{Ae} = \mathbf{R}. \quad (32)$$

In equation (32), \mathbf{e} is the discretization error vector, because the components of the vector are alternatively given by the approximation errors of the expansion coefficients, $(U_i - \tilde{U}_i)$ and $(Q_i - \tilde{Q}_i)$. This equation thus justifies the estimation of the discretization error using the residual vector \mathbf{R} . \mathbf{A} is the same coefficient matrix as that of equation (19). Moreover, the components R_i of the residual vector \mathbf{R} are defined by

$$R_i = -\frac{1}{2} \int_{\Gamma} w_i(u - \check{u}) d\Gamma - \int_{\Gamma} w_i \int_{\Gamma} q^*(u - \check{u}) d\Gamma^2 + \int_{\Gamma} w_i \int_{\Gamma} u^*(q - \check{q}) d\Gamma^2, \quad (33)$$

$$(i = 1, 2, \dots, N),$$

where the true value of $(u - \check{u})$ and $(q - \check{q})$ cannot be given in general cases, and then the components R_i ($i = 1, 2, \dots, N$) are evaluated approximately.

4 Determination of optimal threshold parameters

As defined above, the optimal threshold parameter prescribes the thresholding value by which the matrix compression yields the coefficient matrix with the least memory requirements without the accuracy reduction in BE solution. In the present paper, we attempt to determine the optimal value for the Beylkin-type matrix compression. To achieve this, we impose the equilibrium of the truncation and discretization errors on BE solution. This is however, only the basic idea for setting the optimal value. We thus introduce several assumptions and approximations together with the error equilibrium, to develop the parameter determination strategy available for practical and engineering BE analysis.

In the optimal parameter setting, we have to ensure the equilibrium of the discretization and truncation errors, at least. This error equivalence is dealt with in terms of their potential components, i.e., $\|\Delta \mathbf{z}_u\| \sim \|\mathbf{e}_u\|$ where a subscript “ u ” represents the potential components of the vectors. This is because boundary integral equation (13) is described in the order of the potential. Moreover, the equilibrium is imposed on the residual norms: $\|\mathbf{A}\Delta \mathbf{z}\| \sim \|\mathbf{A}\mathbf{e}\|$. Then, we assume that the error equilibrium $\|\Delta \mathbf{z}_u\| \sim \|\mathbf{e}_u\|$ is not violated when the residual norms satisfy the relation $\|\mathbf{A}\Delta \mathbf{z}\| \sim \|\mathbf{A}\mathbf{e}\|$. Considering the residual norm equilibrium, we require the following relation:

$$\frac{\|\mathbf{A}\Delta \mathbf{z}\|}{\|\mathbf{u}\|} = \frac{\|\mathbf{A}\mathbf{e}\|}{\|\mathbf{u}\|} = \frac{\|\mathbf{R}\|}{\|\mathbf{u}\|}, \quad (34)$$

in the case of matrix compression using the optimal thresholding value. In implementation of the present determination strategy, the components of the residual vector \mathbf{R} are approximated by

$$R_i \simeq c_i, \quad (35)$$

$$c_i = -\frac{1}{2} \int_{\Gamma} w_i(\hat{u} - \tilde{u}) d\Gamma - \int_{\Gamma} w_i \int_{\Gamma} q^*(\hat{u} - \tilde{u}) d\Gamma^2, \quad (i = 1, 2, \dots, N), \quad (36)$$

where \hat{u} is a higher-order interpolation of \tilde{u} . We now define \hat{u} by the scaling functions $\phi_{m_r+2,i}$ ($i = 1, 2, \dots, N + n_{m_r+1}$) at the level $(m_r + 2)$ as

$$\hat{u} = \sum_{i=1}^{N+n_{m_r+1}} \hat{U}_i \phi_{m_r+2,i}. \quad (37)$$

Hence, equation (34) is rewritten as

$$\frac{\|\mathbf{A}\Delta \mathbf{z}\|}{\|\mathbf{u}\|} = \frac{\|\mathbf{c}\|}{\|\mathbf{u}\|}. \quad (38)$$

In equation (38), if we attempt to evaluate the true value of $\|\mathbf{c}\|/\|\mathbf{u}\|$, we have to calculate the BE solution \tilde{u} as shown in equation (14): \tilde{u} is just the BE solution on main analysis. This pre-processing — evaluation of $\|\mathbf{c}\|/\|\mathbf{u}\|$ — requires large computational cost comparable to that of main BE analysis, and is impractical. The residual norm $\|\mathbf{c}\|/\|\mathbf{u}\|$ may however, usually have the asymptotical convergence like the BE solution,

because this norm indicates the discretization error. We thus introduce the following approximation to evaluate the value of $\|\mathbf{c}\|/\|\mathbf{u}\|$:

$$\frac{\|\mathbf{c}\|}{\|\mathbf{u}\|} \simeq \alpha \cdot N^{-\beta}, \quad (39)$$

where the constants α and β are independent of the DOF. In the present strategy, we determine the values of α and β using BE solutions. Note that these solutions are obtained under the same boundary conditions as that of main analysis, but have smaller DOFs than \tilde{u} . The smaller DOFs of the solutions are obviously advantageous to save the additional computational work.

Next, let us derive the relation between the truncation error and the optimal threshold parameter, from the right-hand side terms of inequality (27). The norms $\|\mathbf{G}\|$, $\|\mathbf{H}\|$, $\|\Delta\mathbf{G}\|$ and $\|\Delta\mathbf{H}\|$, which are estimated in the sense of maximum norm, are bounded as follows:

$$\|\mathbf{G}\|_\infty \leq C_1, \quad \|\mathbf{H}\|_\infty \leq C_2, \quad \|\Delta\mathbf{G}\|_\infty \leq C_3, \quad \|\Delta\mathbf{H}\|_\infty \leq C_4, \quad (40)$$

where the constants C_1 , C_2 , C_3 and C_4 are independent of DOF. The proof of equation (40) is lengthy, and is thus omitted. In what follows, the norm $\|\cdot\|$ implies the maximum norm $\|\cdot\|_\infty$.

Based on inequality (40), we propose the following relation from inequality (27):

$$\begin{aligned} \frac{\|\mathbf{A}\Delta\mathbf{z}\|}{\|\mathbf{u}\|} &\approx \|\mathbf{H}\| \left(\frac{\Delta G_{max}}{G_{max}} + \frac{\Delta H_{max}}{H_{max}} \right) \approx \|\mathbf{H}\|(\eta_g + \eta_h), \\ \Delta G_{max} &:= \max_{i,j=1,\dots,N} |\Delta g_{ij}| \approx \eta_g \cdot G_{max}, \\ \Delta H_{max} &:= \max_{i,j=1,\dots,N} |\Delta h_{ij}| \approx \eta_h \cdot H_{max}, \end{aligned} \quad (41)$$

where Δg_{ij} and Δh_{ij} are the entries of the matrices $\Delta\mathbf{G}$ and $\Delta\mathbf{H}$, respectively.

As shown in equation (41), the threshold parameters η_g and η_h indicate the contributions of truncation error concerning the matrices \mathbf{G} and \mathbf{H} to the residual norm $\|\mathbf{A}\Delta\mathbf{z}\|$, respectively. Hence, it is rational to set η_g and η_h to a thresholding value: $\eta_g = \eta_h = \eta_{opt}$. Then, the first equation in (41) can be rewritten by

$$\frac{\|\mathbf{A}\Delta\mathbf{z}\|}{\|\mathbf{u}\|} \approx 2\eta_{opt}\|\mathbf{H}\|. \quad (42)$$

where η_{opt} is the optimal threshold parameter.

Substituting equations (38) and (39) into equation (42), we have

$$\alpha \cdot N^{-\beta} \simeq 2\eta_{opt}\|\mathbf{H}\|. \quad (43)$$

In the above equations, $\|\mathbf{H}\|$ is the norm of the $N \times N$ matrix \mathbf{H} with the same DOF as that of main BE analysis; evaluation of $\|\mathbf{H}\|$ requires generation of all the entries of $N \times N$ matrix. We thus approximate $\|\mathbf{H}\|$ by

$$\|\mathbf{H}\| \simeq \|\tilde{\mathbf{H}}\|, \quad (44)$$

where $\bar{\mathbf{H}}$ is the coefficient matrix \mathbf{H} that is generated to determine the constants α and β in equation (39). The size of the matrix $\bar{\mathbf{H}}$ is set to substantially smaller than that of the matrix \mathbf{H} , in implementation of the determination procedure. The computational work for evaluating the norm $\|\bar{\mathbf{H}}\|$ will thus become small in comparison with that of the main BE analysis.

From equations (42), (43) and (44), *a priori* estimation of the optimal threshold parameter is derived from equations (43) and (44) as follows:

$$\eta_{opt} = \frac{\alpha N^{-\beta}}{2\|\bar{\mathbf{H}}\|}. \quad (45)$$

In the present determination strategy, *a priori* estimation (45) is derived by imposing several assumptions and approximations on error equilibrium (38). These will be verified through numerical experiments in Section 6.

5 Non-zero entries of coefficient matrices

The matrix compression based on the Beylkin-type algorithm ensures $O(N \log N)$ non-zero entries of the $N \times N$ coefficient matrix [12]. Indeed, the amount of storage of quasi-linear order results from the use of fixed thresholding value independently of DOF; the threshold parameter determined by the present strategy possesses the DOF dependency, in order to preserve the accuracy. In the situation in which a coefficient matrix is compressed using such optimal thresholding value, $O(N \log N)$ non-zero entries of the compressed matrix may not be obtained. In the present section, we thus estimate the number of non-zero entries of the coefficient matrices that are compressed by the truncation strategy described in Section 2.3 and with the optimal threshold parameter.

We count the number of non-zero entries of matrices \mathbf{G} and \mathbf{H} . Using Schwab's technique [10], this estimation can be carried out in the same manner independently of the kinds of the matrices. We hence show the details of estimation corresponding to the matrix \mathbf{G} alone.

The non-zero entries of $\tilde{\mathbf{G}}$ defined as the compressed matrix of \mathbf{G} are counted in every submatrices as follows:

$$\tilde{\mathbf{G}} := \mathbf{G} + \Delta\mathbf{G}, \quad \tilde{\mathbf{G}} = \begin{bmatrix} \tilde{\mathbf{G}}_{\phi\phi} & \tilde{\mathbf{G}}_{\phi\psi} \\ \tilde{\mathbf{G}}_{\psi\phi} & \tilde{\mathbf{G}}_{\psi\psi} \end{bmatrix}, \quad (46)$$

where $\Delta\mathbf{G}$ is the matrix assembled by the truncated entries Δg_{ij} of the matrix \mathbf{G} . Moreover, the subscripts “ ϕ ” and “ ψ ” represent the kinds of basis used for generation of their entries. For example, “ $\psi\psi$ ” indicates that two basis functions w_i and w_j are wavelets both. \mathbf{G} and $\tilde{\mathbf{G}}$ are $N \times N$ matrices: the DOF of BE solution, N , is defined by

$$N := n_s + \sum_{k=0}^{m_r} n_k, \quad (47)$$

where n_s and n_k are the numbers of scaling functions and wavelets in the level k , respectively. In equation (47), we assume that $n_k := 2^k \cdot n_s$. Then, $N = 2^{m_r+1} \cdot n_s$.

In the present truncation strategy, all the entries of $\tilde{\mathbf{G}}_{\phi\phi}$ are stored. This is because these entries have only the same decay with respect to the distance $\bar{r} := \text{dist}(\text{supp } w_i, \text{supp } w_j)$ as that in the conventional BE analysis. The number of entries of $\tilde{\mathbf{G}}_{\phi\phi}$, $\mathcal{N}(\tilde{\mathbf{G}}_{\phi\phi})$, is thus estimated as follows:

$$\mathcal{N}(\tilde{\mathbf{G}}_{\phi\phi}) = n_s^2. \quad (48)$$

Next, let us count the number of the entries of $\tilde{\mathbf{G}}_{\phi\psi}$ and $\tilde{\mathbf{G}}_{\psi\phi}$. Since \mathbf{G} and $\tilde{\mathbf{G}}$ are symmetric matrices, the submatrices $\tilde{\mathbf{G}}_{\psi\phi}$ and $\tilde{\mathbf{G}}_{\phi\psi}$ have the same number of non-zero entries. i.e.,

$$\mathcal{N}(\tilde{\mathbf{G}}_{\phi\psi}) = \mathcal{N}(\tilde{\mathbf{G}}_{\psi\phi}). \quad (49)$$

We thus demonstrate the estimation of $\mathcal{N}(\tilde{\mathbf{G}}_{\phi\psi})$ below.

By dividing $\tilde{\mathbf{G}}_{\phi\psi}$ into the submatrices $\tilde{\mathbf{G}}_{\phi\psi}^{(k_j)}$ ($k_j = 0, 1, \dots, m_r$), we have

$$\mathcal{N}(\tilde{\mathbf{G}}_{\phi\psi}) := \sum_{k_j=0}^{m_r} \mathcal{N}(\tilde{\mathbf{G}}_{\phi\psi}^{(k_j)}), \quad (50)$$

where $\tilde{\mathbf{G}}_{\phi\psi}^{(k_j)}$ is the submatrix corresponding to the resolution level k_j . The number of non-zero entries of each submatrix $\tilde{\mathbf{G}}_{\phi\psi}^{(k_j)}$, $\mathcal{N}(\tilde{\mathbf{G}}_{\phi\psi}^{(k_j)})$, is bounded by

$$\begin{aligned} \mathcal{N}(\tilde{\mathbf{G}}_{\phi\psi}^{(k_j)}) &\leq n_s \left(\frac{1+2\delta}{2^{-k_j}} + 1 \right) = n_s \cdot 2^{k_j} \left(1 + 2^{-k_j} + 2\delta \right), \\ \delta &:= \min_{i,j=1,2,\dots,N} \left\{ \bar{r} := \text{dist}(\text{supp } w_i, \text{supp } w_j) \right\}. \end{aligned} \quad (51)$$

From equations (20) and (22), δ is given by

$$\delta \sim \eta^{-\frac{1}{n}} \left(\frac{G_{max}}{C_g} \right)^{-\frac{1}{n}} 2^{-\frac{2n+1}{2n}k_j}, \quad (52)$$

where n is the order of the vanishing moments.

In the matrix compression scheme with the present determination strategy, the threshold parameter η has the following DOF dependency:

$$\eta \sim C' N^{-\beta}, \quad (\beta > 0). \quad (53)$$

Substituting equation (53) into (52), we have

$$\delta \sim C \cdot 2^{-\frac{2n+1}{2n}k_j} N^{\frac{\beta}{n}}. \quad (54)$$

We now substitute equation (54) into (51), and sum up $\mathcal{N}(\tilde{\mathbf{G}}_{\phi\psi}^{(k_j)})$ with respect to k_j . As a result, $\mathcal{N}(\tilde{\mathbf{G}}_{\phi\psi})$ is bounded as follows:

$$\begin{aligned} \mathcal{N}(\tilde{\mathbf{G}}_{\phi\psi}) &\leq n_s \sum_{k_j=0}^{m_r} \left(1 + 2^{-k_j} + 2C \cdot 2^{-\frac{2n+1}{2n}k_j} N^{\frac{\beta}{n}} \right) 2^{k_j} \\ &\leq C_1 \left(N + \log N + N^{\frac{\beta}{n}} \right), \end{aligned} \quad (55)$$

where the constant C_1 is independent of N and m_r .

Finally, let us consider the submatrix $\tilde{\mathbf{G}}_{\psi\psi}$. The number of the non-zero entries of $\tilde{\mathbf{G}}_{\psi\psi}$, $\mathcal{N}(\tilde{\mathbf{G}}_{\psi\psi})$, is defined by

$$\mathcal{N}(\tilde{\mathbf{G}}_{\psi\psi}) := \sum_{k_i=0}^{m_r} \sum_{k_j=0}^{m_r} \mathcal{N}(\tilde{\mathbf{G}}_{\psi\psi}^{(k_i, k_j)}), \quad (56)$$

where $\tilde{\mathbf{G}}_{\psi\psi}^{(k_i, k_j)}$ is the submatrix of which the resolution levels of two basis functions w_i and w_j are k_i and k_j .

The non-zero entries of the submatrix $\tilde{\mathbf{G}}_{\psi\psi}^{(k_i, k_j)}$ can be counted as follows:

$$\mathcal{N}(\tilde{\mathbf{G}}_{\psi\psi}^{(k_i, k_j)}) \leq n_s \cdot 2^{k_i+k_j} \left(2^{-k_i} + 2^{-k_j} + 2\delta \right). \quad (57)$$

In inequality (57), δ is derived from equations (20), (22) and (53) as

$$\delta \sim C \cdot 2^{-\frac{2n+1}{4n}(k_i+k_j)} N^{\frac{\beta}{2n}}. \quad (58)$$

Substituting equations (57) and (58) into (56), we can obtain the following estimation of $\mathcal{N}(\tilde{\mathbf{G}}_{\psi\psi})$:

$$\begin{aligned} \mathcal{N}(\tilde{\mathbf{G}}_{\psi\psi}) &\leq n_s \sum_{k_i=0}^{m_r} \sum_{k_j=0}^{m_r} 2^{k_i+k_j} \left(2^{-k_i} + 2^{-k_j} + 2C \cdot 2^{-\frac{2n+1}{4n}(k_i+k_j)} N^{\frac{\beta}{2n}} \right) \\ &\leq C_2 \left(N \log N + N^{1+\frac{\beta-1}{2n}} \right). \end{aligned} \quad (59)$$

From equation (48), (49), (55) and (59),

$$\begin{aligned} \mathcal{N}(\tilde{\mathbf{G}}) &= \mathcal{N}(\tilde{\mathbf{G}}_{\phi\phi}) + 2\mathcal{N}(\tilde{\mathbf{G}}_{\phi\psi}) + \mathcal{N}(\tilde{\mathbf{G}}_{\psi\psi}) \\ &\leq CN \left(N^{\frac{\beta}{n}-1} + N^{\frac{\beta-1}{2n}} + \log N \right). \end{aligned} \quad (60)$$

As shown in equation (60), $\mathcal{N}(\tilde{\mathbf{G}})$ has the following asymptotic order dependently on β :

$$\mathcal{N}(\tilde{\mathbf{G}}) = \begin{cases} O(N \log N), & 0 < \beta < 1, \\ O(N^{1+\gamma_1}), & 1 \leq \beta < 2n-1, \\ O(N^{1+\gamma_2}), & \beta \geq 2n-1, \end{cases} \quad (61)$$

$$\gamma_1 := \min \left\{ 1, \frac{\beta-1}{2n} \right\}, \quad \gamma_2 := \min \left\{ 1, \frac{\beta}{n} - 1 \right\}.$$

The number of the stored entries of the matrix $\tilde{\mathbf{H}} := \mathbf{H} + \Delta\mathbf{H}$, $\mathcal{N}(\tilde{\mathbf{H}})$, can be estimated in the same manner as estimation of $\mathcal{N}(\tilde{\mathbf{G}})$. i.e.,

$$\mathcal{N}(\tilde{\mathbf{H}}) = \begin{cases} O(N^{1+\gamma_3}), & 0 < \beta \leq \frac{(2n+1)^2}{2n}, \\ O(N^{1+\gamma_4}), & \beta > \frac{(2n+1)^2}{2n}, \end{cases} \quad (62)$$

$$\gamma_3 := \min \left\{ 1, \frac{\beta}{2n+1} \right\}, \quad \gamma_4 := \min \left\{ 1, \frac{2\beta - 2n - 1}{2(n+1)} \right\}.$$

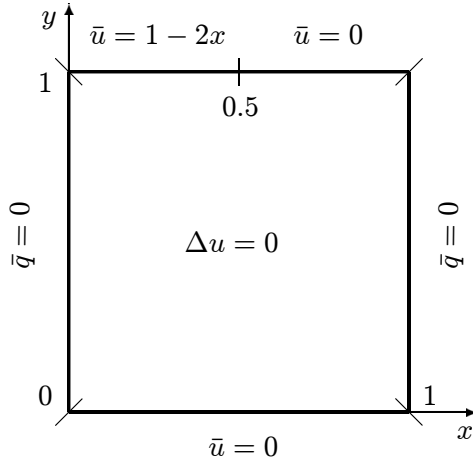


Figure 1: Boundary conditions in the numerical example.

6 Numerical results

In this section, we attempt to verify several assumptions and approximations, which are introduced to set the optimal threshold parameter, through numerical experiments. We chose the two-dimensional problem with simple boundary shapes as a test problem. Figure 1 shows the boundary conditions of the test problem. Note that this problem has the true solution u as

$$u(x, y) = \frac{1}{4}y + \frac{4}{\pi^2} \sum_{n=1}^{\infty} \frac{1}{n^2 \sinh n\pi} \left(1 - \cos \frac{n\pi}{2}\right) \cos n\pi x \cdot \sinh n\pi y, \quad (63)$$

and the solution shows the singularity on $\partial u / \partial n$ at $(1/2, 1)$ and $(0, 1)$.

This example is not the typical problem that computational cost of BE analysis is substantially reduced with the wavelet BEM. However, the present numerical experiments will perform their roles as the benchmark tests for proving the present scheme the effective determination strategy of the optimal threshold parameter, sufficiently. This is because most of assumptions and approximations introduced in Section 4 are concerned with the treatment of norm or the error equilibrium.

In the present experiments, we employed two kinds of spline wavelets — the Haar wavelets ($m = 0, n = 1$) and the piecewise linear non-orthogonal wavelets with second-order vanishing moments ($m = 1, n = 2$) — as basis function. The wavelet expansion for approximating the potential or the flux on the boundary is defined in every interval corresponding to $n_b (= 5)$ subboundaries. The DOF is set to $N = n_b \cdot 2^{m_r+1}$ (Haar) or $N = n_b \cdot (2^{m_r+2} + 1)$ (piecewise linear). Moreover, the constants α and β in equation (39) were estimated using the BE solutions with 40 and 80 DOFs (Haar wavelets), and 45 and 85 DOFs (piecewise linear wavelets). The entries of the coefficient matrix were generated through analytical integration.

6.1. Verification of basic assumptions

In the error estimation for determining the optimal threshold parameter, we have introduced the following assumptions:

- (i) $\eta_g = \eta_h = \eta_{opt}$.
- (ii) $\|\mathbf{A}\Delta\mathbf{z}\| \sim \|\mathbf{A}\mathbf{e}\| \sim \|\mathbf{c}\|$ is equivalent to $\|\mathbf{e}_u\| \sim \|\Delta\mathbf{z}_u\|$, for truncation under the optimal threshold parameters.
- (iii) $\frac{\|\mathbf{A}\Delta\mathbf{z}\|}{\|\mathbf{u}\|} \approx \|\mathbf{H}\| \left(\frac{\Delta G_{max}}{G_{max}} + \frac{\Delta H_{max}}{H_{max}} \right) \approx \|\mathbf{H}\|(\eta_g + \eta_h)$, in the sense of maximum norm.

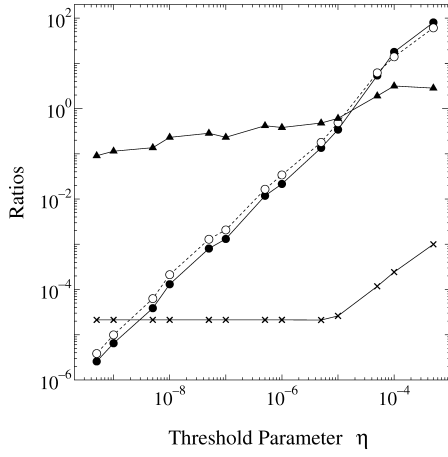
To verify these assumptions, we monitor the relation between the threshold parameter η and three ratios $\|\mathbf{A}\Delta\mathbf{z}\|/\|\mathbf{c}\|$, $\|\Delta\mathbf{z}_u\|/\|\mathbf{e}_u\|$ and $\|\mathbf{A}\Delta\mathbf{z}\|/(\eta\|\mathbf{H}\| \cdot \|\mathbf{u}\|)$. Figure 2 depicts the results for these ratios. In this figure, we also show the error norm $\|\mathbf{u}_{exact} - \mathbf{u}\|$ where \mathbf{u}_{exact} is the vector corresponding to the expansion coefficients of the true solution u . Note that in the present experiments the matrices \mathbf{G} or \mathbf{H} were alternatively compressed in order to discuss the validity of assumptions (i) and (iii).

Let us first consider assumption (i). As shown in Figure 2, $\|\mathbf{u}_{exact} - \mathbf{u}\|$ has the point at which the level of the error norm begins to increase. The value of η at the point is the optimal value of the threshold parameter, and this value is independent of the kind of the compressed matrix. Assumption (i), $\eta_g = \eta_h = \eta_{opt}$, is thus a practical and rational choice of the threshold parameter in wavelet-based BE analysis.

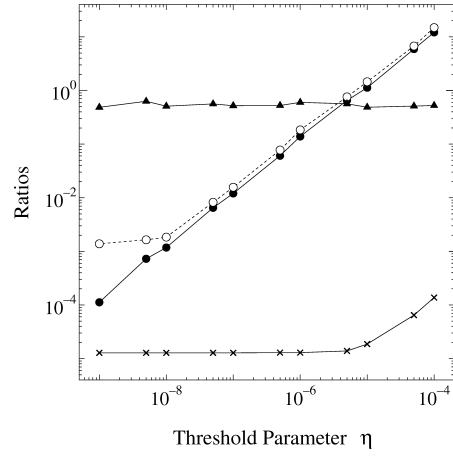
Assumption (ii) can be verified from the ratios $\|\mathbf{A}\Delta\mathbf{z}\|/\|\mathbf{c}\|$ and $\|\Delta\mathbf{z}_u\|/\|\mathbf{e}_u\|$. For all examples, the value of two ratios are nearly equal, except that the threshold parameter is substantially small. Consequently, the norm equivalences $\|\mathbf{A}\Delta\mathbf{z}\| \sim \|\mathbf{c}\|$ and $\|\Delta\mathbf{z}_u\| \sim \|\mathbf{e}_u\|$ are simultaneously satisfied, and then the threshold parameter η has the optimal value. Hence, it is valid to employ $\|\mathbf{A}\Delta\mathbf{z}\| \sim \|\mathbf{c}\|$ instead of the error equilibrium $\|\Delta\mathbf{z}_u\| \sim \|\mathbf{e}_u\|$, as the condition for determining the optimal threshold parameter η_{opt} .

Next, we discuss the validity of assumption (iii) based on the results for the ratio $\|\mathbf{A}\Delta\mathbf{z}\|/(\eta\|\mathbf{H}\| \cdot \|\mathbf{u}\|)$. This is because for alternative compression of \mathbf{G} or \mathbf{H} it is needed to hold $\|\mathbf{A}\Delta\mathbf{z}\|/\|\mathbf{u}\| \sim \|\mathbf{H}\|(\eta_g + \eta_h) \sim \eta\|\mathbf{H}\|$ in order to determine the optimal thresholding value. As shown in Figure 2, $\|\mathbf{A}\Delta\mathbf{z}\|/(\eta\|\mathbf{H}\| \cdot \|\mathbf{u}\|)$ is nearly equal to unity at the optimal value of η in all the examples. Since $\|\mathbf{A}\Delta\mathbf{z}\|/(\eta\|\mathbf{H}\| \cdot \|\mathbf{u}\|) \sim 1$ is equivalent to $\|\mathbf{A}\Delta\mathbf{z}\|/\|\mathbf{u}\| \sim \eta\|\mathbf{H}\|$, assumption (iii) is valid.

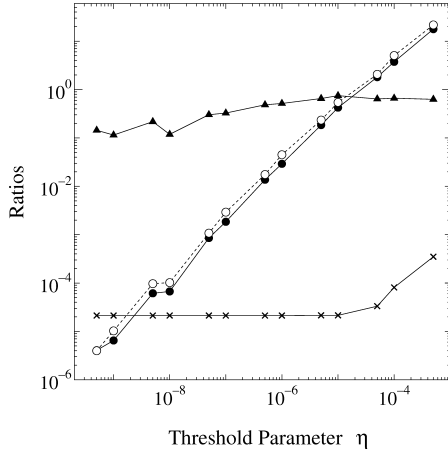
The above verification is based on the numerical results obtained using the true value of $\|\mathbf{H}\|$. In determination process of the optimal threshold parameter, the norm $\|\mathbf{H}\|$ is however, approximated by $\|\mathbf{H}\| \simeq \|\bar{\mathbf{H}}\|$ where $\bar{\mathbf{H}}$ is the H-matrix of the BE equation used to generate the approximate expression of $\|\mathbf{c}\|/\|\mathbf{u}\|$. We should thus discuss the validity of this approximation. Figure 3 shows the relation between the DOF and the ratio $\|\bar{\mathbf{H}}\|/\|\mathbf{H}\|$. The ratio $\|\bar{\mathbf{H}}\|/\|\mathbf{H}\|$ varies with the rate of $O(N^{-\mu})$ where $\mu \geq 0$ has very small value. This implies that the difference between the true value $\|\mathbf{H}\|$ and the approximation $\|\bar{\mathbf{H}}\|$ remains small independently of the DOF. We can hence conclude that



(i) Compression for the matrix \mathbf{G} alone.

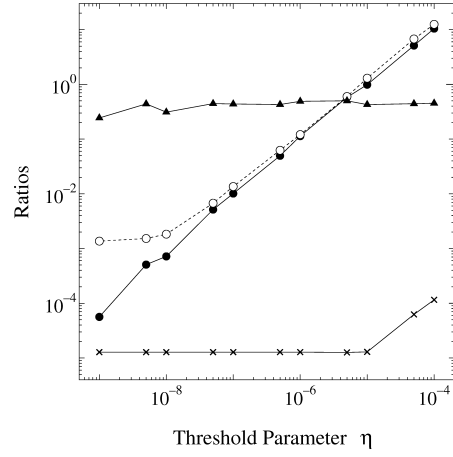


(i) Compression for the matrix \mathbf{G} alone.



(ii) Compression for the matrix \mathbf{H} alone.

(a) Haar wavelets. (2,560 DOFs)



(ii) Compression for the matrix \mathbf{H} alone.

(b) Piecewise linear wavelets. (2,565 DOFs)

Figure 2: Valiation of three kinds of ratios $\|\mathbf{A}\Delta\mathbf{z}\|/\|\mathbf{c}\|$, $\|\Delta\mathbf{z}_u\|/\|\mathbf{e}_u\|$ and $\|\mathbf{A}\Delta\mathbf{z}\|/(\eta\|\mathbf{H}\|\cdot\|\mathbf{u}\|)$. The matrices \mathbf{G} or \mathbf{H} were alternatively compressed. ((a): Haar wavelets (2,560 DOFs), (b): piecewise linear wavelets (2,565 DOFs), \bullet : $\|\mathbf{A}\Delta\mathbf{z}\|/\|\mathbf{c}\|$, \circ : $\|\Delta\mathbf{z}_u\|/\|\mathbf{e}_u\|$, \blacktriangle : $\|\mathbf{A}\Delta\mathbf{z}\|/(\eta\|\mathbf{H}\|\cdot\|\mathbf{u}\|)$, \times : $\|\mathbf{u}_{exact} - \mathbf{u}\|$)

$\|\bar{\mathbf{H}}\|$ provides a good approximation of $\|\mathbf{H}\|$. In this situation, the above discussion may be consistent even if $\|\mathbf{H}\|$ is replaced by $\|\bar{\mathbf{H}}\|$.

6.2. Accuracy of optimal threshold parameter

We now investigate the accuracy of the optimal threshold parameter determined by the present strategy. Figure 4 depicts the relation between the DOF and the norm $\|\mathbf{c}\|/\|\mathbf{u}\|$, and the optimal values of the threshold parameter. In this figure, we also plot the optimal values searched through repetition of numerical experiments: the experimental value is denoted by $\eta^{(exp)}$.

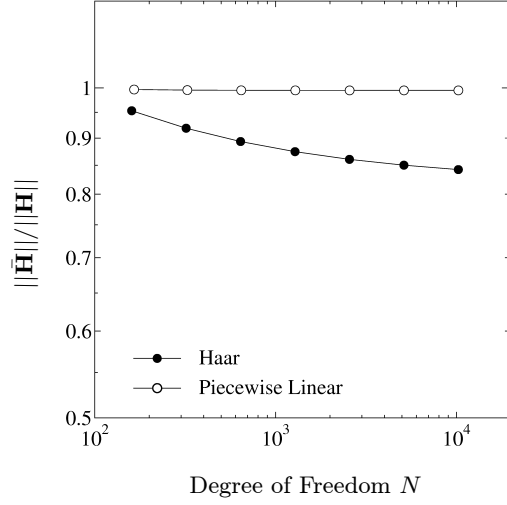


Figure 3: Relation between DOFs and $\|\bar{\mathbf{H}}\|/\|\mathbf{H}\|$. $\|\bar{\mathbf{H}}\|$ is evaluated using the numerical solution with 80 ($m_r = 3$, Haar wavelets) or 85 ($m_r = 2$, piecewise linear wavelets) DOFs.

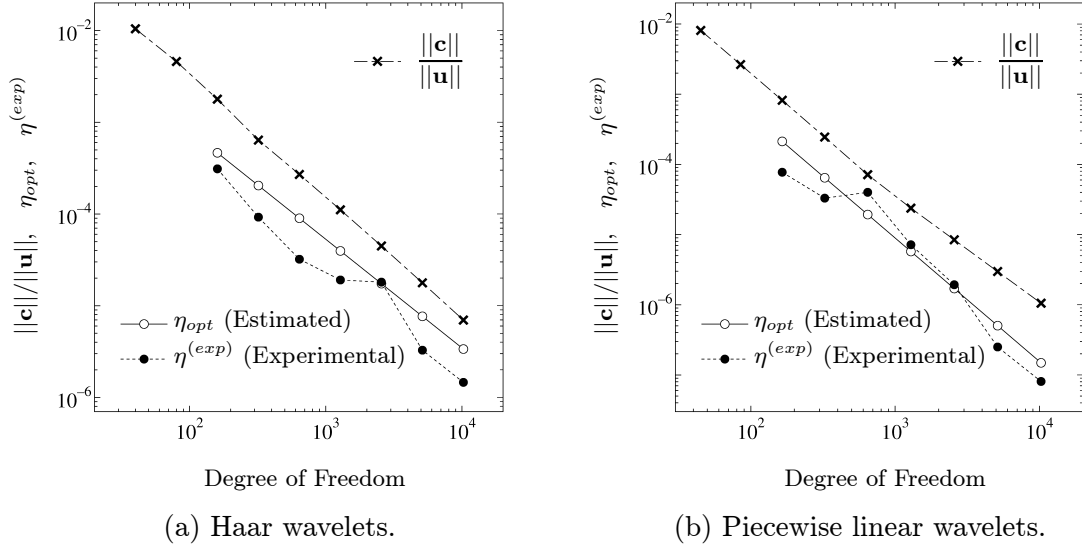


Figure 4: The optimal threshold parameters estimated by the present strategy. (\circ : the estimated value η_{opt} (by equation (45)), \bullet : the experimental value $\eta^{(exp)}$ (determined through repetition of numerical experiments), \times : $\|\mathbf{c}\|/\|\mathbf{u}\|$)

In derivation of estimation (45) from truncation error estimation (27), we assumed that

$$\frac{\|\mathbf{A}\Delta\mathbf{z}\|}{\|\mathbf{u}\|} \approx \|\mathbf{H}\| \left(\frac{\Delta G_{max}}{G_{max}} + \frac{\Delta H_{max}}{H_{max}} \right) \approx \|\mathbf{H}\|(\eta_g + \eta_h) \approx 2\eta_{opt}\|\mathbf{H}\|.$$

This assumption that has already been verified in the previous subsection implies that the optimal threshold parameter η_{opt} has the same asymptotical order as the residual norm $\|\mathbf{c}\|/\|\mathbf{u}\|$. In other words, the estimated threshold parameter shows $\eta_{opt} \sim O(N^{-\beta})$ where β is the asymptotical convergence rate of $\|\mathbf{c}\|/\|\mathbf{u}\|$. The validity of this approximation,

Table 1: Error of the potential $\|\mathbf{u} - \mathbf{u}_{exact}\|$. (“ $\eta = \eta^{(exp)}$ ” indicates the results for the experimental values $\eta^{(exp)}$). (a): Haar wavelets, (b): piecewise linear wavelets)

(a) Haar wavelets.			(b) Piecewise linear wavelets.		
N	Error of the potential		N	Error of the potential	
	$(\eta = \eta_{opt})$	$(\eta = \eta^{(exp)})$		$(\eta = \eta_{opt})$	$(\eta = \eta^{(exp)})$
160	9.639×10^{-3}	9.526×10^{-3}	165	1.350×10^{-2}	1.342×10^{-2}
320	5.499×10^{-3}	5.464×10^{-3}	325	6.592×10^{-3}	6.481×10^{-3}
640	3.090×10^{-3}	3.091×10^{-3}	645	3.081×10^{-3}	3.043×10^{-3}
1,280	1.768×10^{-3}	1.729×10^{-3}	1,285	1.311×10^{-3}	1.319×10^{-3}
2,560	9.661×10^{-4}	9.604×10^{-4}	2,565	4.547×10^{-4}	4.551×10^{-4}
5,120	5.374×10^{-4}	5.535×10^{-4}	5,125	1.120×10^{-4}	1.283×10^{-4}

$\eta_{opt} \sim O(N^{-\beta})$, can be verified by comparing the asymptotical order of $\|\mathbf{c}\|/\|\mathbf{u}\|$ (or η_{opt}) with that of $\eta^{(exp)}$.

As shown in Figure 4, the asymptotical order of the experimental value $\eta^{(exp)}$ is roughly equal to β , though the value of $\eta^{(exp)}$ is fluctuating. On the other hand, the residual norm $\|\mathbf{c}\|/\|\mathbf{u}\|$ decreases uniformly with increasing DOF. The uniform convergence of $O(N^{-\beta})$ is indicated independently of the number of degrees of freedom, and hence we can easily evaluate the value of $\|\mathbf{c}\|/\|\mathbf{u}\|$ by the approximation $\|\mathbf{c}\|/\|\mathbf{u}\| \sim \alpha \cdot N^{-\beta}$. In the present example, the constants α and β used in the approximate expression were determined by the BE solutions with $N = 30 - 100$. The DOF $N = 30 - 100$ corresponds to the DOF with the finest resolution level m_r of 1 – 3. Hence, we will be able to estimate the optimal threshold parameter at smaller additional work in engineering applications of the wavelet BEM.

Next, let us consider the reliability of equation (45). The estimated value η_{opt} by equation (45) tends to be slightly larger than the value of $\eta^{(exp)}$, as shown in Figure 4. In the present matrix compression, the use of larger value of the threshold parameter leads to a highly compressed coefficient matrix. We may however, encounter the increase in the error of BE solution. To investigate the influences of the matrix compression using the estimated optimal value η_{opt} on the error of BE solution, we tabulate the errors of the potential, $\|\mathbf{u} - \mathbf{u}_{exact}\|$, in Table 1. Even if the estimated value η_{opt} is set to a larger value than the experimental value $\eta^{(exp)}$, the error for $\eta = \eta_{opt}$ is roughly equal to that for $\eta = \eta^{(exp)}$. We can thus conclude that the matrix compression using the estimated optimal threshold parameter scarcely cause the accuracy reduction of BE solution.

6.3. Performance of BE analysis

Figure 5 depicts the number of non-zero entries of the matrices \mathbf{G} and \mathbf{H} . Notice that in the present experiment Haar wavelets ($n = 1$) were used as basis functions. The residual norm $\|\mathbf{c}\|/\|\mathbf{u}\|$ in the test problem has an asymptotical order of $\beta = 1.32$, i.e., $O(N^{-1.32})$,

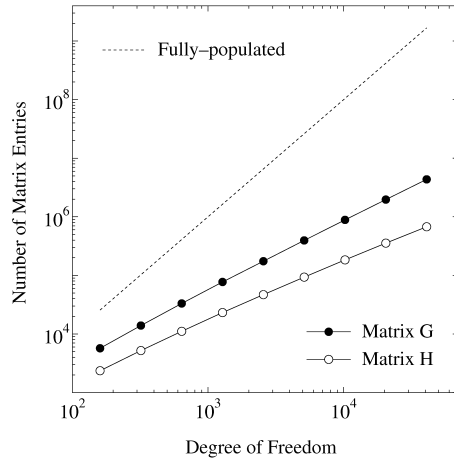


Figure 5: The number of non-zero entries of the compressed matrices $\tilde{\mathbf{G}}$ and $\tilde{\mathbf{H}}$. In the present experiment, the Haar wavelets were used as the basis functions. The asymptotical convergence rate of the residual norm $\|\mathbf{c}\|/\|\mathbf{u}\|$ is then $O(N^{-1.32})$. The numerical results show $\mathcal{N}(\tilde{\mathbf{G}}) \sim O(N^{1.19})$ and $\mathcal{N}(\tilde{\mathbf{H}}) \sim O(N^{1.02})$, whereas using the estimation presented in Section 5 $\mathcal{N}(\tilde{\mathbf{G}})$ and $\mathcal{N}(\tilde{\mathbf{H}})$ were estimated at $O(N^{1.18})$ and $O(N^{1.40})$, respectively.

Table 2: Compression rate of the coefficient matrices \mathbf{G} and \mathbf{H} .

(a) Haar wavelets.			(b) Piecewise linear wavelets.		
N	\mathbf{G} (%)	\mathbf{H} (%)	N	\mathbf{G} (%)	\mathbf{H} (%)
160	22.258	9.211	165	14.718	13.051
320	13.613	5.086	325	8.948	7.124
640	8.098	2.712	645	5.468	3.827
1,280	4.713	1.415	1,285	3.257	2.002
2,560	2.662	0.716	2,565	1.896	1.016
5,120	1.507	0.356	5,125	1.103	0.510
10,240	0.844	0.175	10,245	0.654	0.253

and then the numbers of the non-zero entries $\mathcal{N}(\tilde{\mathbf{G}})$ and $\mathcal{N}(\tilde{\mathbf{H}})$ are estimated as $O(N^{1.18})$ and $O(N^{1.40})$, respectively, with equations (61) and (62). On the other hand, the numerical results also show $O(N^\gamma)$; $\gamma = 1.19$ ($\mathcal{N}(\tilde{\mathbf{G}})$) and $\gamma = 1.02$ ($\mathcal{N}(\tilde{\mathbf{H}})$). Overestimation of $\mathcal{N}(\tilde{\mathbf{H}})$ with equation (62) will be caused by the fact that in the present estimation the null entries concerning the kernel $q^* = 0$ on a straight line are counted as non-zero entries.

The compression rates of the matrices \mathbf{G} and \mathbf{H} are tabulated in Table 2. The rate of compression of $N \times N$ matrix was evaluated by

$$(\text{Compression Rate})(\%) := 100 \times \frac{(\text{Number of Stored Entries})}{N^2}.$$

In these examples, the stored entries of \mathbf{G} and \mathbf{H} are reduced to about 1 – 5 % for

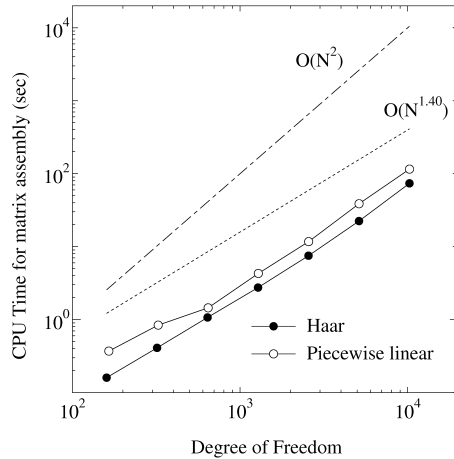


Figure 6: The CPU time for matrix assembly. This computation time does NOT include the CPU time for determining the optimal value η_{opt} . In the present experiments, 0.37 (Haar) and 1.39 (piecewise linear) seconds were spent in estimation of η_{opt} . (\bullet : Haar wavelets, \circ : Piecewise linear wavelets)

$N = 1,000 - 2,000$. As mentioned above, the matrix compression based on the present truncation scheme leads to $O(N^{1+\gamma})$ non-zero entries, not to $O(N(\log N)^a)$ ($a \geq 0$); we can expect to substantially save the memory requirements in practical BE analysis.

Figure 6 shows the CPU time for matrix assembly. Note that the indicated results in this figure does not include the computational time for determining the optimal threshold parameter. The CPU time also increases $O(N^{\bar{\gamma}})$ ($1 \leq \bar{\gamma} < 2$) with DOFs like the number of non-zero entries. The rates are both $O(N^{1.40})$ independently of the kinds of wavelets, and indeed these are roughly equal to the estimation of $\mathcal{N}(\tilde{\mathbf{H}})$ (the number of non-zero entries of $\tilde{\mathbf{H}}$). We can derive the following two conclusions from this fact: (i) the CPU time can be reduced by using *a priori* truncation scheme described in Section 2 and avoiding the integrations concerning the truncated entries, and (ii) for the present numerical tests the *a priori* estimation carried out to all the matrix entries does not cause the obvious increase in the amount of computational work. On the other hand, the additional CPU time for determining η_{opt} was 0.37 (Haar) or 1.39 (piecewise linear) seconds. In the present examples, these are comparable to the total CPU time for $N = 300 - 500$; are only about 10 % of the CPU time for $N \simeq 2,000$.

7 Concluding remarks

We have proposed a practical determination strategy of the optimal threshold parameter for matrix compression in the wavelet BEM. In the present paper, we have discussed the thresholding value for the Beylkin-type truncation algorithm, which have been widely used in the engineering analyses with the wavelet BEM. The optimal threshold parameter is used in matrix compression to reduce the memory requirement and the computational

work as much as possible with the accuracy of BE solution preserving. We have determined such value as in BE solution the truncation error is comparable to the discretization error. The both errors are estimated in the residual sense. The estimation of the discretization error is carried out using the potential contributions $\|\mathbf{c}\|$ in the residual vector \mathbf{R} , whereas the truncation error is estimated by the truncation contribution $\|\mathbf{A}\Delta\mathbf{z}\|$ in the residual on boundary element equations. In the determination of the optimal value, we have imposed $\|\mathbf{A}\Delta\mathbf{z}\|/\|\mathbf{u}\| \sim \|\mathbf{c}\|/\|\mathbf{u}\|$ on the residual norms. The equilibrium of the residuals plays the most important role in the present determination strategy, nevertheless, the true value of $\|\mathbf{c}\|/\|\mathbf{u}\|$ corresponding to the DOF of main BE analysis cannot be evaluated without solving the boundary element equation in the main analysis. We have thus attempted to estimate the value of $\|\mathbf{c}\|/\|\mathbf{u}\|$ using the approximation $\alpha N^{-\beta}$, and then the approximate expression is developed by the BE solutions with smaller DOFs. Furthermore, several assumptions and approximations have been introduced to determine the optimal threshold parameter, and have been verified through numerical experiments.

As shown in Section 6, the matrix compression using the optimal threshold parameter generates a sparse coefficient matrix with $O(N^{1+\gamma})$ ($0 \leq \gamma < 1$) non-zero-entries. This is because we use the Beylkin-type truncation scheme and then require the equilibrium of the truncation and discretization errors. We cannot consequently obtain the computational complexity and memory requirements of quasi-linear order, like Dahmen-Schwab truncation algorithm. On the other hand, the amount of storage can be substantially reduced by the present compression scheme: in the examples shown in the preceding section we obtained a few percent compression rates for the DOF $N \sim 1,000$. These results however, seem to be not sufficient to ascertain whether Beylkin-type truncation reduces a large amount of computational cost comparable to that for Schwab-type compression or not. We hope to present the numerical comparison with the alternative (quasi-optimal) compression scheme in future.

To determine the optimal value of the threshold parameter, we have to calculate BE solutions with smaller DOFs than that of main analysis. This computation obviously requires additional computational work. When we are obliged to deal with large DOFs such as 3-D problems or 2-D problems with complicated boundaries, the additional work may require large computational cost. In this situation, a number of scaling functions without vanishing moments is a cause of increasing the computational cost of wavelet-based BE analysis. Hence, the reduction of such computations is an important issue of rather the wavelet BEM than the present determination strategy including subsidiary calculation with smaller DOFs.

References

- [1] Goswami JC, Chen AK, Chui CK. On solving first-kind integral equations using wavelets on a bounded interval. *IEEE Transactions on Antennas and Propagation* 1995; 43(6): 614–622.
- [2] Rathsfeld A. A wavelet algorithm for the boundary element solution of a geodetic

- boundary value problem. *Computer Methods in Applied Mechanics and Engineering* 1998; 157: 267–287.
- [3] Lage C, Schwab C. Wavelet Galerkin algorithms for boundary integral equations. *SIAM Journal on Scientific Computing* 1999; 20(6): 2195–2222.
- [4] Koro K, Abe K. Non-orthogonal spline wavelets for boundary element analysis. *Engineering Analysis with Boundary Elements* 2001; 25: 149–164.
- [5] Rokhlin V. Rapid solution of integral equations of classical potential theory. *Journal of Computational Physics* 1983; 60: 187–207.
- [6] Greengard L, Huang J, Rokhlin V, Wandzura S. Accelerating fast multipole methods for the Helmholtz equation at low frequencies. *IEEE Computational Science & Engineering* 1998; 5(3): 32–38.
- [7] Dahmen W, Prösdorff S, Schneider R. Wavelet approximation methods for pseudodifferential equations II: Matrix compression and fast solution. *Advances in Computational Mathematics* 1993; 1: 259–335.
- [8] von Petersdorff T, Schwab C, Schneider R. Multiwavelets for second-kind integral equations. *SIAM Journal on Numerical Analysis* 1997; 34(6): 2212–2227.
- [9] Schneider R. Multiskalen- und wavelet- matrixkompression: Analysisbasierte methoden zur effizienten Lösung großer vollbesetzter gleichungssysteme. *Advances in Numerical Mathematics*, B.G. Teubner, Stuttgart, Germany, 1998. (in German)
- [10] von Petersdorff T, Schwab C. Wavelet approximations for first kind boundary integral equations on polygons. *Numerische Mathematik* 1996; 74: 479–519.
- [11] von Petersdorff T, Schwab C. Fully discrete Galerkin BEM. in *Multiresolution Analysis and Partial Differential Equations*, W. Dahmen, P. Kurdila and P. Oswald, eds., *Wavelet Analysis and its applications*, Academic Press, Germany, 1997: 287–346.
- [12] Beylkin G, Coifman R, Rokhlin V. Fast wavelet transform and numerical algorithm I. *Communications on Pure and Applied Mathematics* 1991; 44: 141–183.
- [13] Steinberg BZ, Leviatan Y. On the use of wavelet expansions in the method of moments. *IEEE Transactions on Antennas and Propagation* 1993; 41: 610–619.
- [14] Sabetfakhri K, Katehi LBP. Analysis of integrated millimeter-wave and submillimeter-wave waveguides using orthonormal wavelet expansions. *IEEE Transactions on Microwave Theory and Techniques* 1994; 42(12): 2412–2422.
- [15] Wang G. A hybrid wavelet expansion and boundary element analysis of electromagnetic scattering from conducting objects. *IEEE Transactions on Antennas and Propagation* 1995; 43(2): 170–178.

- [16] Koro K, Abe K, Tazaki H. Application of discrete wavelet transform to wavelet collocation BEM. *Journal of Applied Mechanics* 1999; 2: 153–162 (in Japanese).
- [17] Abe K, Koro K. Gauss quadrature method using wavelet basis as a weighting function for boundary element analysis. *Boundary Elements XXIII*, Beskos DE, Brebbia CA, Katsikadelis JT, Manolis GD, eds., WIT Press, Southampton, Boston 2001: 455-464.
- [18] Abe K. A new residue and nodal error evaluation in h-adaptive boundary element method. *Advances in Engineering Software* 1992; 15: 231–239.
- [19] Abe K, Koro K, Itami K. An h-hierarchical Galerkin BEM using Haar wavelets. *Engineering Analysis with Boundary Elements* 2001; 25: 581–591.